Journal of Magnetic Resonance 192 (2008) 235–243

Contents lists available at ScienceDirect

Journal of Magnetic Resonance

journal homepage: www.elsevier.com/locate/jmr

Linear phase slope in pulse design: Application to coherence transfer

Naum I. Gershenzon [a], Thomas E. Skinner [a,*], Bernhard Brutscher [c], Navin Khaneja [d], Manoj Nimbalkar [b], Burkhard Luy [b], Steffen J. Glaser [b]

[a] Department of Physics, The Wright State University, 3640 Colonel John F. Glenn Highway, Dayton, OH 45435-0001, USA
[b] Department of Chemistry, Technische Universität München, 85747 Garching, Germany
[c] Institute de Biologie Structurale Jean-Pierre Ebel, CNRS-CEA-UJF, 41 rue Jules Horowitz, 38027 Grenoble, France
[d] Division of Applied Sciences, Harvard University, Cambridge, MA 02138, USA

ARTICLE INFO

Article history:
Received 2 November 2007
Revised 22 February 2008
Available online 8 March 2008

Keywords:
Optimal control theory
Phase slope
Coherence transfer
Relaxation

ABSTRACT

Using optimal control methods, robust broadband excitation pulses can be designed with a defined linear phase dispersion. Applications include increased bandwidth for a given pulse length compared to equivalent pulses requiring no phase correction, selective pulses, and pulses that mitigate the effects of relaxation. This also makes it possible to create pulses that are equivalent to ideal hard pulses followed by an effective evolution period. For example, in applications, where the excitation pulse is followed by a constant delay, e.g. for the evolution of heteronuclear couplings, part of the pulse duration can be absorbed in existing delays, significantly reducing the time overhead of long, highly robust pulses. We refer to the class of such excitation pulses with a defined linear phase dispersion as ICEBERG pulses (Inherent Coherence Evolution optimized Broadband Excitation Resulting in constant phase Gradients). A systematic study of the dependence of the excitation efficiency on the phase dispersion of the excitation pulses is presented, which reveals surprising opportunities for improved pulse sequence performance.

1. Introduction

The fundamental goal of pulse sequence design is to control spin trajectories. Although the ideal final state of the sample magnetization just prior to acquisition may be obvious for a given application, how to achieve this state can be less obvious. Optimal control theory [1] is a powerful method which can be applied to this problem. It has been used, for example, to derive ultra-broadband excitation pulses, BEBOP [2–6], which are tolerant to RF inhomogeneity/miscalibration and require no phase correction. This imposes a rather stringent requirement on the optimal control algorithm—for a range of possible RF calibrations, it must drive all spins within the desired range of resonance offsets to the same final state. Yet, a linear phase dispersion in the final magnetization as a function of offset is readily corrected in many practical applications utilizing, for example, hard pulses or Gaussian pulses [7].

We have formerly compared BEBOP performance (no phase correction required) to a phase-corrected hard pulse, since this is an excellent benchmark for broadband excitation. BEBOP pulses are exceptional by this standard, but a fairer comparison would entail optimized pulses that can be phase-corrected, also. We therefore consider the advantages of allowing this increased flexibility in pulse design.

The slope of the phase as a function of offset appears to be an important parameter for pulse design. Applications include increased bandwidth for a given pulse length compared to equivalent pulses requiring no phase correction (or, shorter pulses for the same bandwidth), selective pulses, and pulses that mitigate the effects of relaxation [8]. We therefore characterize the values of the phase slope that are attainable for excitation pulses. We find a new class of pulses with smoothly modulated amplitude that depend in a predictable fashion on specific parameters of the pulse design. We also present an application to coherence transfer. In particular, we consider pulses for coherence transfer that make it possible to absorb some of the evolution time for heteronuclear couplings into the excitation pulse. One can then utilize specific performance benefits of relatively long pulses without adding significantly to the experiment time.

2. Phase slope

We are interested in controlling the phase, φ, that the transverse magnetization, M_{xy}, acquires during a pulse of length T_p. The phase is measured here from the x-axis. Requiring the slope of the phase to be constant as a function of resonance offset ω (units of radians/s) gives a linear phase for M_{xy}, which is desirable for many applications. The particular value for the slope, $\partial\varphi/\partial\omega$, then requires some elaboration.

* Corresponding author. Fax: +1 937 775 2222.
E-mail address: thomas.skinner@wright.edu (T.E. Skinner).

1090-7807/$ - see front matter © 2008 Elsevier Inc. All rights reserved.
doi:10.1016/j.jmr.2008.02.021

In the absence of the pulse, the phase acquired by M_{xy} at offset ω during time T_p due to chemical-shift evolution is ωT_p, so the slope is equal to T_p. We define a normalized, dimensionless phase slope

$$R = (1/T_p)\partial\varphi/\partial\omega. \quad (1)$$

Values of R at each offset characterize the phase relative to the maximum phase that could be produced solely by chemical-shift evolution during the time T_p. A pulse that produces focused magnetization of fixed phase for all spins in the offset range of interest would have a constant $R = 0$ (i.e., a self-refocused pulse). BEBOP pulses obtained to date are typically $R \approx 0$ pulses. We recently considered, in the context of relaxation effects, the design of pulses with the equivalent phase slope of a hard pulse [8]. The desired slope is obtained from a hard pulse phase slope (equal to $2/\pi$ on resonance), scaled according to Eq. (1) by t_{90}/T_p, where t_{90} is the length of the hard pulse. As expected, there was a considerable performance advantage for such pulses compared to $R = 0$.

Selective pulses found in the literature to date are commonly $R = 1/2$ pulses [7,9–13]. The symmetry of the resulting pulse provides an advantage in the development of various algorithms used in selective pulse design, such as Shinnar–Le Roux [10], inverse scattering [11], polychromatic [12], and stereographic projection [13]. In fact, the standard form of the SLR algorithm [10] can only generate linear phase of this value. Algorithms for selective pulses which produce more general linear phase are described in the literature [14], but no practical pulses are provided to characterize performance or demonstrate precisely what is possible for general R, except for $R = 0$ [11]. Although this topic is beyond the scope of the present article, it illustrates the relevance of phase slope to selective pulses.

Another important example of the utility of the phase slope is presented by the equivalence of chemical-shift and coupling evolution of an irradiated spin. During the pulse, the effect of the coupling J (in radians/s) on the irradiated spins at a chemical-shift offset ω is simply an additional offset $\pm J/2$ for the ± orientation of the spins. Thus, if the irradiated spins at all offsets in a range of interest are transformed to the same state so that $R = 0$ independent of offset, there is no net J-evolution at the end of the pulse. A different but related definition with relevance to spin decoupling has been presented by Waugh [15]. Conversely, if the chemical-shift evolution of the irradiated spins during a pulse of length T_p is the same as the chemical-shift evolution during a delay of the same length ($R = 1$ for all offsets), the coupling evolution is the undiminished value $(J/2)T_p$. For constant R (i.e., linear phase slope) in the range $0 < R < 1$, partial coupling evolution occurs. In addition, $R < 0$ would generate magnetization of reverse phase that would refocus after a delay RT_p.

Applications and the range of R attainable in practice are discussed further in what follows.

3. Optimal control algorithm

The optimal control methodology has been described in detail previously [2–6]. It was used to calculate what are referred to here as $R = 0$ pulses, which transform initial z magnetization to the x-axis for any offset and RF calibration within the design specifications. For excitation of transverse magnetization of phase slope R, we now consider separate target states for each offset of the form

$$\vec{F} = [\cos(\varphi), \sin(\varphi), 0]. \quad (2)$$

Choosing $\varphi = R(\omega T_p)$ gives a linear phase slope, which is our focus here, but any function can be considered for its potential to define a useful target phase, making the method completely general.

We have previously input random noise for the initial RF used to start the algorithm. Characterizing the performance of various modifications and additions to the algorithm was an important goal, and we wanted to avoid imposing any bias on what might constitute the best final solution. Inputting noise also served to demonstrate the power and efficiency of optimal control, showing that it is not necessary to guess an approximate solution in order for the algorithm to either converge or converge in a useable time frame, which is often the case in standard optimization routines. Some of the resulting pulses look very much like noise themselves, although their outstanding performance demonstrates they are not at all random.

Now that the algorithm is well-established, we turn to the derivation of smooth pulse shapes. We start the algorithm with an initial RF pulse of constant small amplitude (approximately zero) and constant phase ($\pi/4$). This results in a class of sinc-like pulse shapes that is reminiscent of, and appears to include, polychromatic pulses [12] as a subset. In addition to being easy to implement on a wide range of spectrometers, the shape of the new pulses depends in a very regular fashion on R for values in the range $0 \leqslant R \leqslant 1$.

4. Pulse characterization

We first investigate the characteristics of $R \geqslant 0$ pulses in some detail before considering also the possibility of pulses with negative phase slope.

4.1. Pulse shape

The pulse shape and performance is a function of a combination of parameters such as pulse width T_p, total offset range Δf (in Hz) covered by the pulse, maximum amplitude, and phase slope R. Pulses were designed to uniformly excite various bandwidths with different combinations of pulse length and values of the phase slope. No limit was set on the RF amplitude during this particular set of optimizations, so that in each case, the maximum RF amplitude of the resulting pulse is the "natural" amplitude A_{max} for the particular combination of Δf, T_p, and R.

For broadband excitation defined only by these parameters, we find a class of purely amplitude-modulated pulses, with A_{max} occurring at time $t_A = (1 - R)T_p$. The pulse shape is reminiscent of a shifted or asymmetric sinc pulse with peak amplitude at t_A. It consists of a number of oscillations equal to $(\Delta f/\ 2)\ T_p$, which increase in amplitude for $t \leqslant t_A$ and decrease for $t \geqslant t_A$. For the approximate range $0.01 < R < 0.99$, we find $A_{max} \approx 0.28\Delta f$. High quality performance requires significantly greater RF power for the demanding cases $R = 0$ and $R = 1$. Representative pulses illustrating these general features are shown in Fig. 1.

The simplest pulse which one could propose to generate a linear phase slope R would do nothing for a time $(1 - R)T_p$, followed by an ideal high power pulse of negligible length to rotate spins of all offsets in the desired bandwidth to the x-axis, followed by chemical-shift precession for the remaining time RT_p, as in

$$(1 - R)T_p - 90_y - RT_p. \quad (3)$$

This is essentially what the pulses of Fig. 1 do, with the sinc-like oscillations providing the modifications that allow more practical values for the maximum RF amplitude compared to the ideal prototype pulse. The small and increasing oscillations in pulse amplitude at the beginning of the pulse (e.g., Fig. 1A–D) fine-tune the orientations of the spins near the z-axis so they can be aligned near the x-axis by the large-amplitude portion of the pulse. During subsequent chemical-shift evolution, residual z magnetization is reduced towards zero by the remaining oscillations.

If we limit the pulse amplitude in the optimization procedure, so that the amplitude can not exceed a given value RF_{lim}, the shape

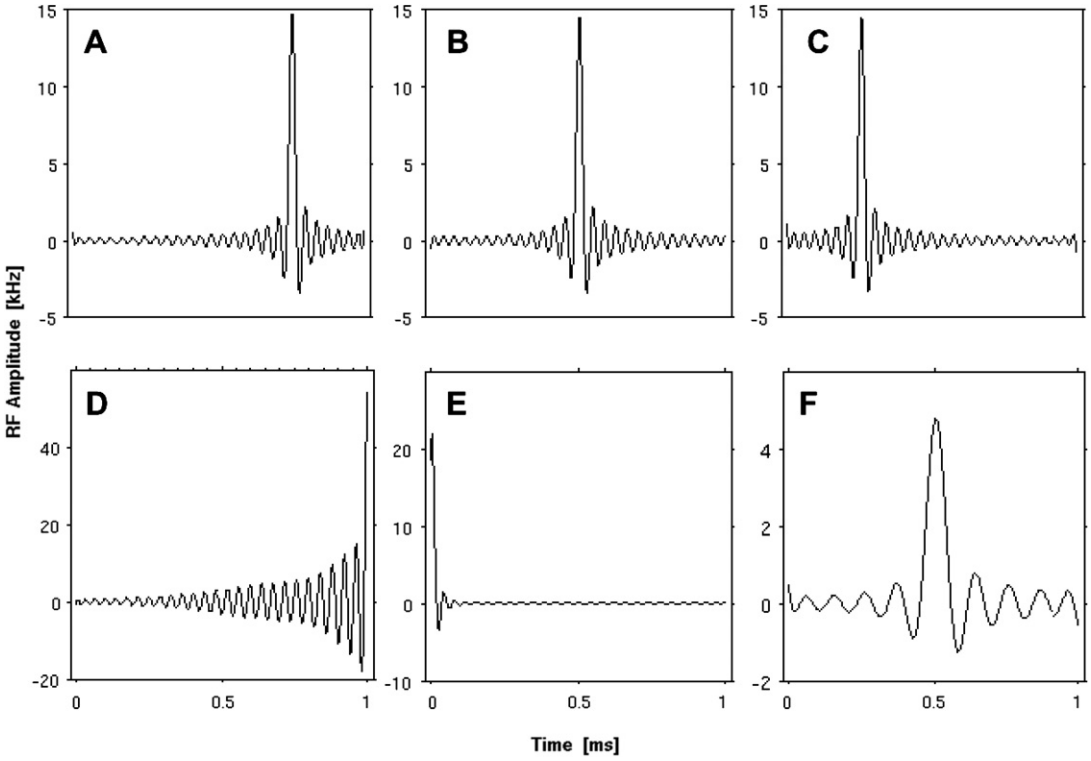

Fig. 1. RF amplitude is plotted as a function of time for a series of 1 ms pulses designed using different combinations of R and bandwidth, Δf. No limit was set on the RF amplitude during the optimization. (A) $R = 0.25$, $\Delta f = 50$ kHz, (B) $R = 0.5$, $\Delta f = 50$ kHz, (C) $R = 0.75$, $\Delta f = 50$ kHz, (D) $R = 0$, $\Delta f = 50$ kHz, (E) $R = 1$, $\Delta f = 50$ kHz, (F) $R = 0.5$, $\Delta f = 20$ kHz.

and performance of the pulse does not change considerably for RF_{lim} 30–40% smaller than A_{max}. The peak amplitude is clipped, and the amplitude of the oscillations increases, as shown in Fig. 2A. Further decreases in RF_{lim} cause corresponding decreases in pulse performance, and the pulse shape becomes more irregular, requiring both phase and amplitude modulation to achieve optimal performance. Phase and amplitude modulation are also required if a wide range of tolerance to RF miscalibration/inhomogeneity is included in the optimization.

High quality pulses are also achievable for $R < 0$. In the ideal case, using high power pulses of negligible length, the well-known solution is to add a refocusing pulse at the end of the sequence in Eq. (3) to obtain, for example,

$$(1 - R)T_p - 90_y - RT_p - 180_x. \quad (4)$$

For more practical, limited values of RF power, we find the same basic structure in the optimized pulses shown in Fig. 3, but the pulse must operate during the delay periods to compensate for the reduced (finite) RF power. The design of finite-power pulses which still achieve the nearly ideal performance of the ideal sequence given in Eq. (4) is not trivial. Moreover, examination of the performance given by the pulse shown in Fig. 3A reveals that it delivers a poor 90° rotation at various offsets followed by a compensating poor 180° rotation to achieve the ideal performance at the end of the pulse. Thus, the entire $90-\Delta-180$ block has been optimized, as opposed to the individual pulses, providing a broader realization of the principle of global compensation considered in composite pulses [16].

In contrast to the positive R pulses, the optimal control algorithm does not automatically produce negative R pulses which

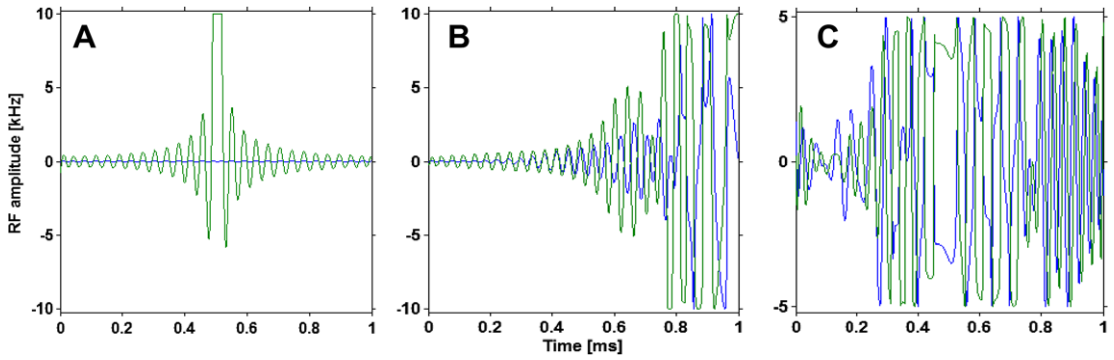

Fig. 2. The x-component (blue) and y-component (green) of RF amplitude are plotted as a function of time for a series of 1 ms pulses designed using different combinations of R and maximum allowed RF amplitude RF_{lim} to excite a bandwidth $\Delta f = 50$ kHz. The "natural" amplitude A_{max} obtained in Fig. 1 without RF clipping is also provided for comparison. (A) $R = 0.5$, $RF_{lim} = 10$ kHz ($A_{max} \approx 14$ kHz), (B) $R = 0$, $RF_{lim} = 10$ kHz ($A_{max} \approx 45$ kHz), (C) $R = 0.5$, $RF_{lim} = 5$ kHz ($A_{max} \approx 14$ kHz). (For interpretation of the references to color in this figure legend, the reader is referred to the web version of this article.)

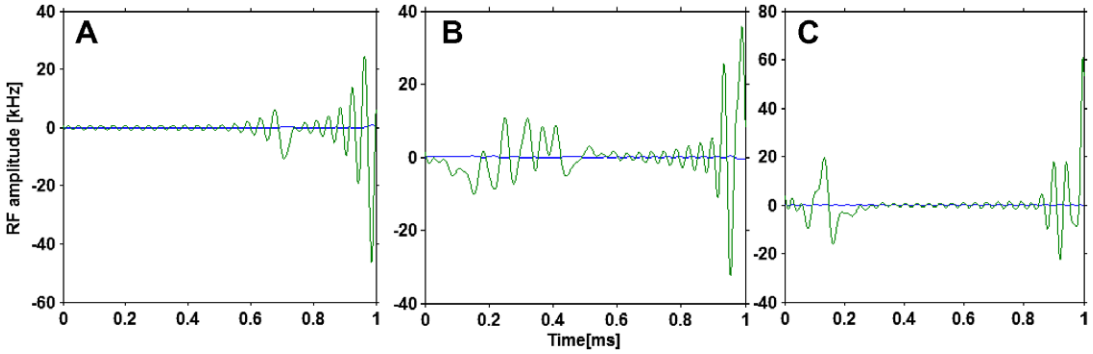

Fig. 3. RF amplitude is plotted as a function of time for a series of 1 ms pulses designed for negative R and excitation bandwidth $\Delta f = 50$ kHz. No limit was set on the RF amplitude during the optimization. (G) $R = -0.25$, (H) $R = -0.5$, (I) $R = -0.75$.

tolerate the same degree of RF field inhomogeneity. Even if a range of RF miscalibration is included in the algorithm, the tolerance to inhomogeneity that can be achieved for the 1 ms pulse length used so far is only about 5%. For negative R, larger pulse length is necessary to achieve the same tolerance to RF inhomogeneity as can be obtained using positive R.

4.2. Pulse performance

The broadband pulses shown in Fig. 1 were designed without considering RF inhomogeneity or miscalibration. Nonetheless, variations in pulse calibration or homogeneity on the order of ±10% have very little effect on performance, as shown in Fig. 4. Contours of transverse magnetization are plotted as functions of resonance offset and peak RF amplitude of the pulse for values of R in the range $0.01 < R < 0.99$. For RF miscalibration/inhomogeneity of ±10%, the transverse magnetization immediately after the pulse exceeds 0.99. Deviations from linearity in the phase are less than 1°–2° over the 50 kHz offset range for miscalibration of ±5%, approaching 3° at RF miscalibrations of ±10%.

4.2.1. Dependence on R and T_p

To more fully characterize the values of linear phase slope that are attainable in practice, we define the quality factor (QF) of a pulse as the value of the transverse magnetization averaged over the target bandwidth of the pulse. Fig. 5 shows four intensity maps of QF as a function of R and T_p corresponding to maximum allowed RF amplitudes of 5 kHz and 15 kHz and a target bandwidth $\Delta f = 50$ kHz. Relaxation effects are considered in the bottom two panels. Each of the 3320 pixels in an image represents the performance of an optimized pulse corresponding to the associated parameters RF_{max}, Δf, T_p, and R. The figure thus represents the design of over 13,000 pulses, providing further testament to the efficiency of the optimal control algorithm.

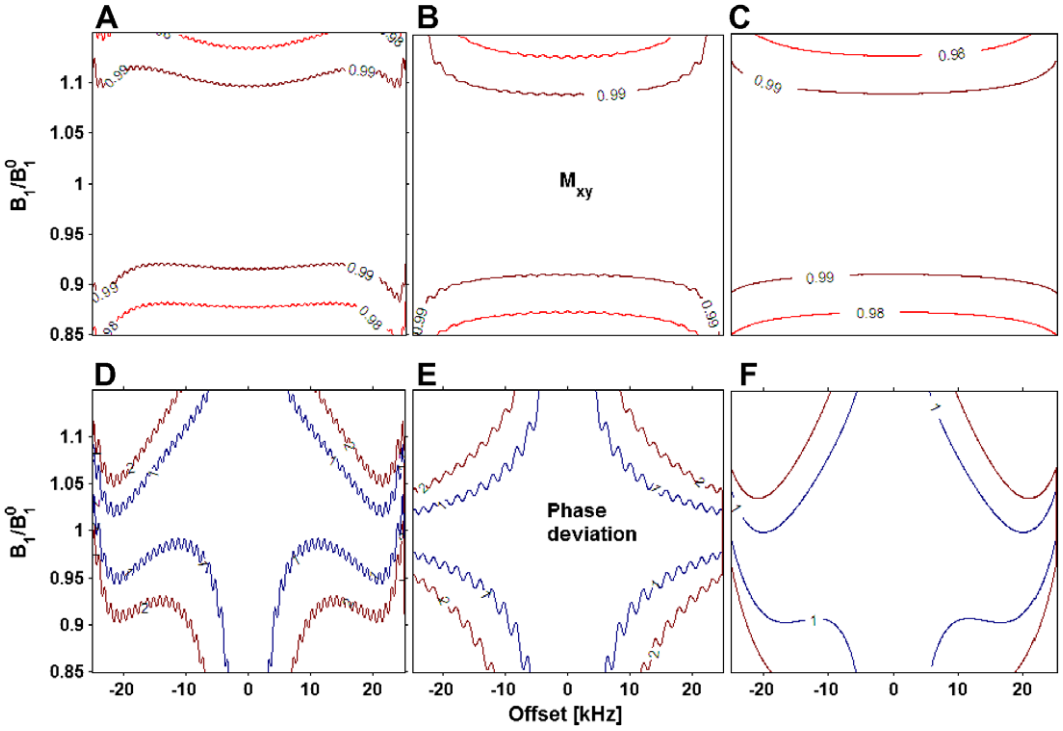

Fig. 4. Transverse magnetization is plotted as a function of resonance offset and peak RF amplitude B_1 obtained by simulating optimized pulses of length $T_p = 1$ ms, target bandwidth $\Delta f = 50$ kHz, and nominal peak amplitude $B_1^0 = 15$ kHz for linear phase slopes (A) $R = 0.01$, (B) $R = 0.5$, and (C) $R = 0.99$, which can be corrected in many applications. Contour lines are [0.99, 0.98]. The deviation in phase from these linear values is shown immediately below in the respective plots (D), (E), and (F) with contours at [1°, 2°]. Only ideal RF values were considered during the optimization procedure, but the resulting pulses are nonetheless tolerant to RF miscalibration/inhomogeneity of approximately ±10%.

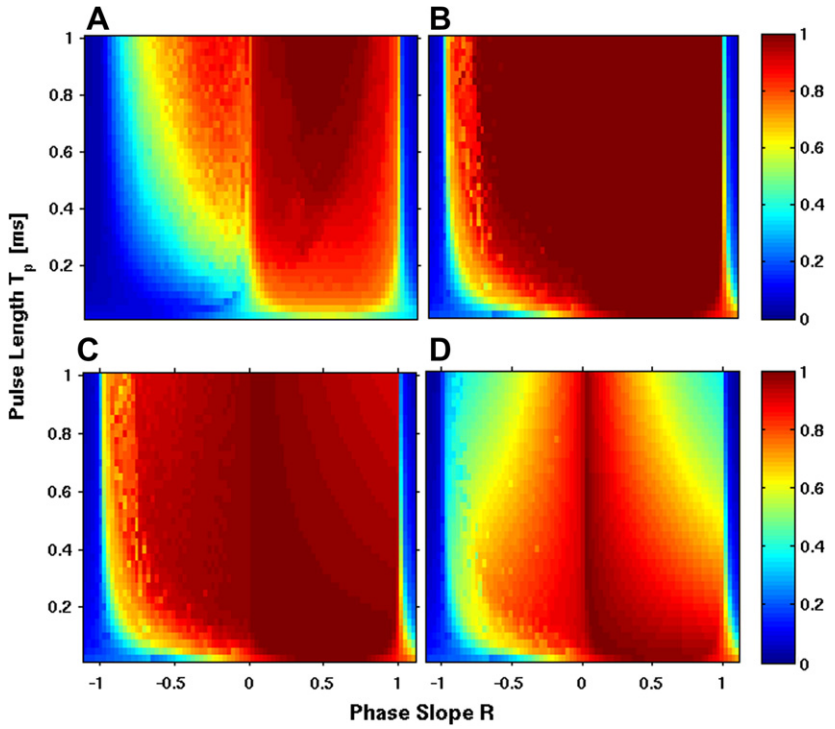

Fig. 5. Quality factor QF for optimal control pulses designed to uniformly excite a bandwidth $\Delta f = 50$ kHz is plotted as a function of T_p and R neglecting relaxation (upper panels) and considering relaxation (lower panels). (A) $RF_{lim} = 5$ kHz. (B) $RF_{lim} = 15$ kHz. (C) $T_1 = T_2 = 10$ ms, $RF_{lim} = 15$ kHz. (D) $T_1 = T_2 = 1$ ms, $RF_{lim} = 15$ kHz. The color bar at the right of the figure provides the scale for QF. Each pixel in the images represents one pulse designed for the respective set of parameters T_p, R, Δf, and maximum allowed amplitude RF_{lim}, resulting in the design of over 13,000 pulses. (For interpretation of the references to color in this figure legend, the reader is referred to the web version of this article.)

In all cases, the value of QF drops to zero for $R > 1$, reflecting the fact that it is not feasible to create an excitation pulse which generates phase slope larger than the chemical-shift precession of transverse magnetization in the absence of the pulse. It is also difficult (but not impossible) to design a high quality pulse ($QF \geqslant 0.99$) for $R < 0$. The apparently anomalous behavior for short T_p near $R = 1$, in which QF increases for the smallest values of T_p, is due to the averaging used to obtain QF. The excitation is very nonuniform at these short pulse lengths, and large values for the transverse magnetization at relatively few offsets compensate in the final average for low values at most offsets. With the exception of these very short pulse lengths, the excitation in other cases is uniform, so QF is a good representation of the transverse magnetization at each offset within the target bandwidth.

Increased bandwidth for a given peak RF amplitude can be achieved using a pulse that produces a linear phase dispersion in the final magnetization as opposed to $R = 0$. This is illustrated in Fig. 5A. A bandwidth of 50 kHz is uniformly excited using a pulse with a peak RF amplitude of only 5 kHz for values of the phase slope centered about $R \approx 1/2$, which requires pulse lengths approximately in the range 0.7–1 ms. If $R = 0$ is required using this peak RF amplitude, the performance of the corresponding pulse over the bandwidth would be much worse for any T_p, as indicated by the lower values of QF. Greater RF power is required to obtain $R \leqslant 0$ and to approach $R = 1$, as shown in Fig. 5B. Peak RF of 30 kHz (not shown) is necessary to achieve values of $R \approx -1$.

The effects of relaxation on the attainable phase slope in the design of relaxation-compensated pulses (RC-BEBOP) [8] are illustrated in Fig. 5C and D. Panel C shows an increasingly restricted range of R values as the pulse length becomes an increasing fraction of the relaxation times $T_1 = T_2 = 10$ ms. For T_p close to $T_1 = T_2 = 1$ ms in panel D, effective RC-BEBOP pulses are of necessity small R pulses. As noted in Ref. [8], the strategy for reducing relaxation effects is to keep the spins close to the z-axis until the end of the pulse, which is achieved for small R pulses of the kind shown in Fig. 1D, irrespective of whether relaxation is explicitly included in the optimization. Including relaxation in the algorithm only produces a signal gain of a few percent at small R, and no gain for larger R. Pulses of the kind shown in Fig. 1 with larger phase slope rotate spins towards the transverse plane earlier in the pulse, producing correspondingly larger losses due to relaxation that cannot be compensated. The $R \approx 0$ BEBOP pulses produced previously without regard to relaxation effects are more complicated and do not keep spins near the z-axis for most of the pulse length. Thus, relaxation–compensation can be significant in these cases [8].

5. Applications

5.1. Shorter broadband excitation

A hard pulse excites transverse magnetization M_{xy} with an approximately linear phase slope ($R = 2/\pi$ on resonance) that can be corrected in many useful applications. Although a hard pulse is probably the workhorse of NMR spectroscopy, neither the excitation profile nor the phase slope are not uniform as a function of resonance offset. At field strengths approaching 1 GHz and typical ^{13}C probe limits on peak RF amplitude of ~15 kHz ($T_p = 16.7$ μs), there is room for improvement, as shown in Fig. 6. An ideally calibrated pulse excites 95% of the attainable transverse magnetization over an offset range of ±17 kHz, and excites less than 90% over ±25 kHz. The phase is linear to within ±2° over the entire offset range of 50 kHz, but can be 3°–4° over large parts of the spectrum, depending on RF inhomogeneity or miscalibration. Accumulated signal losses can be significant when large pulse trains are applied.

Previously, we derived a relatively short 125 μs pulse requiring no phase correction ($R = 0$) that uniformly excites 99% magnetiza-

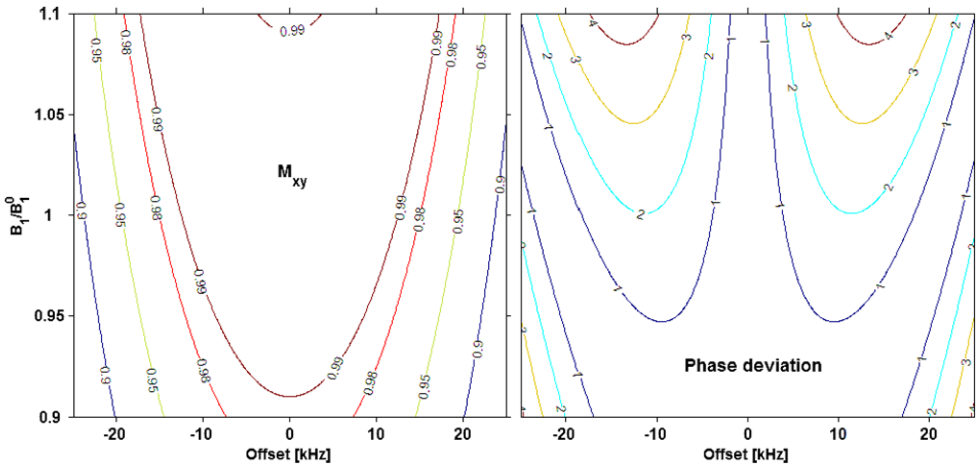

Fig. 6. Performance of a 16.7 μs hard pulse, peak RF amplitude $B_1^0 = 15$ kHz. Transverse magnetization M_{xy} (left panel) and absolute value of the phase deviation from linearity (right panel) are plotted as functions or resonance offset and RF miscalibration/inhomogeneity B_1/B_1^0.

tion over 50 kHz bandwidth with tolerance to RF inhomogeneity of ±10% [5]. If the pulse is no longer required to be self-refocused, we find the 39 μs, $R = 1/2$ pulse shown in Fig. 7. The excited M_{xy} is greater than 0.99 over the entire 50 kHz bandwidth used in the optimization, and also provides tolerance to RF miscalibration of ±7% (>98% for ±10% miscalibration). Deviations in phase linearity (absolute value) are less than 1° over most of the optimization window of ±25 kHz offset and ±10% RF inhomogeneity, rising to 3°–4° only at the extreme edges of the window.

5.2. Coherence transfer

Consider the basic element of a coherence transfer experiment shown in Fig. 8A, a 90° pulse followed by a delay of length τ.

For a pulse that produces a linear phase slope in the transverse magnetization, the parameter R can be interpreted as the fraction of the pulse length in which the net chemical-shift (or coupling) evolution occurs, as discussed in Section 2. Hence, a pulse of phase slope R and duration T_p produces the same phase evolution that would occur for transverse magnetization during a time-delay interval

$$T_{evol} = RT_p, \tag{5}$$

as illustrated in Fig. 8B. The remaining fraction of the pulse can be represented by a 90° excitation pulse of length

$$T_{exc} = T_p - T_{evol} = (1 - R)T_p, \tag{6}$$

in which no phase evolution occurs. Thus, the total time for the $90° - \tau$ element of the sequence can be reduced by the time T_{evol}.

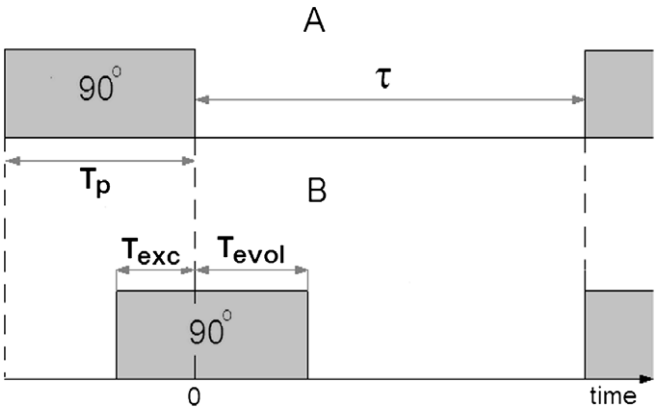

Fig. 8. The use of a linear phase slope pulse to reduce the delay τ in selective coherence transfer in the case where T_p is relatively long. (A) $R = 0$, requiring $\tau = 1/(2J)$. (B) $R > 0$, with $T_{evol} = RT_p$ resulting in chemical-shift evolution ωT_{evol} during the pulse and thus a coupling evolution $(J/2)T_{evol}$, reducing the delay correspondingly. The pulse can be represented by excitation with no phase evolution during the time T_{exc} followed by free precession during T_{evol}.

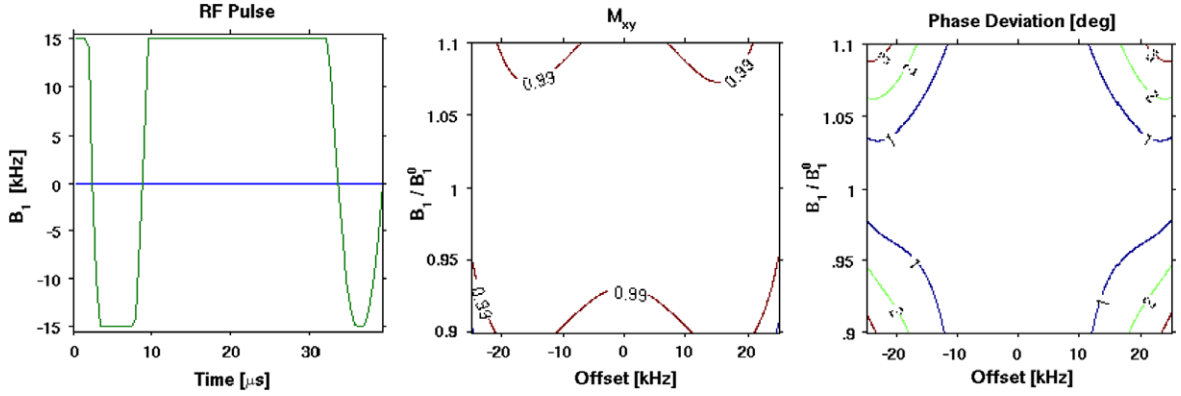

Fig. 7. Amplitude-modulated pulse of length 39 μs and peak RF amplitude $B_1^0 = 15$ kHz, optimized to excite transverse magnetization M_{xy} with linear phase slope $R = 1/2$ over resonance offsets of 50 kHz. The pulse serendipitously provides significant tolerance to RF miscalibration B_1/B_1^0 with small phase deviations (absolute value) from linearity, as shown in the middle and right panels. The 50 kHz, ±10% RF miscalibration window used for the simulations shows $M_{xy} > 0.99$ and phase deviations less than 1° over most of these ranges, with deviations of 3° at the extreme offsets and miscalibrations at the corners of the window.

The performance advantages of certain kinds of longer pulses, such as BEBOP or selective pulses, can then be more fully exploited if they are designed with large R to avoid increasing the experiment time to an unsatisfactory degree. This interpretation of R also provides additional insight into relaxation-compensated pulses, which can be idealized as excitation with no relaxation during T_{exc} followed by chemical-shift evolution and relaxation during T_{evol}.

For the parameters $\Delta f = 50$ kHz, $RF_{lim} = 15$ kHz of Fig. 5B, high performance pulses (QF > 0.99) with $R = 0.975$ are possible for $T_p = 0.2$ ms or greater, giving T_{exc} as small as 5 μs from Eq. (6). A more complete map of QF as a function of R and T_{exc} is shown in Fig. 9. The case $\Delta f = 50$ kHz, $RF_{lim} = 10$ kHz is also provided, showing that high QF > 0.99 and large $R = 0.975$ are still possible, but the minimum value for T_{exc} increases to 10 μs (corresponding to $T_p = 0.4$ ms). In all cases, there is little further improvement to be gained by longer T_p, while shorter T_p decreases performance, so there is an optimal choice of T_p, and hence, T_{exc}, for a given set of parameters.

Relaxation-compensated pulses provide little benefit for this application. The class of linear phase pulses we have presented are naturally compensated for relaxation by choosing small R. As noted, there is only a few percent gain in signal if relaxation is explicitly included in the optimization algorithm for these pulses. There is no difference in performance by including relaxation in the optimization at larger R, and this application demands large R to minimize T_{exc} and the total time for the experiment. Moreover, the signal loss during the τ-delay is unavoidable, no matter what value of R we choose. For example, if there was no relaxation during an ideal $R = 0$ pulse, then $T_{exc} = T_p$, followed by decay for the period τ. If we consider an ideal $R = 1$ pulse, so that $T_{exc} = 0$, we would have the same decay during the time τ, since $R = 1$ ideally rotates all spins to the x-axis instantaneously, followed by chemical-shift evolution and T_2 losses during $T_{evol} = T_p$ and the remainder of the τ-delay. For any other R, we have partial decay during the pulse plus decay during $\tau - T_{evol}$ that gives the same total loss as for the ideal $R = 0$ and $R = 1$ cases, because the partial decay can be considered to occur over a time T_{evol}. Thus, to minimize T_{exc}, we are free to choose the largest R possible for a given acceptable quality factor, independent of relaxation.

More quantitatively, consider the quality factor QF for the pulse of Fig. 5D, showing the effects of relaxation. For a given (positive) R, the pulse extends into the delay period for a time T_{evol}, as shown in Fig. 8B. At the same point in the delay of Fig. 8A, an ideal excitation pulse ($QF_{ideal} = 1$) also would have relaxed for a time T_{evol}, resulting in a signal magnitude $\exp(-T_{evol}/T_2)$ at that time. For later times, the relaxation is the same in both cases. In Fig. 10, we plot the ratio $QF/\exp(-T_{evol}/T_2)$ calculated from Fig. 5D for the signal of the optimized pulse compared to an ideal excitation pulse. For almost any value $R > 0$, the ratio is 1. Only for $R \approx 0$ are there gains of a few percent in using a relaxation-compensated pulse, but small R is of no use in this application. Practically speaking, to minimize T_{exc}, we are free to choose the largest R possible for a given quality factor, independent of relaxation.

5.2.1. Experimental

The viability of employing relatively long ICEBERG pulses with improved excitation profile compared to a hard pulse is illustrated in Fig. 11, using a ^{13}C excited and detected HMQC experiment as an example. Although this experiment would realistically be

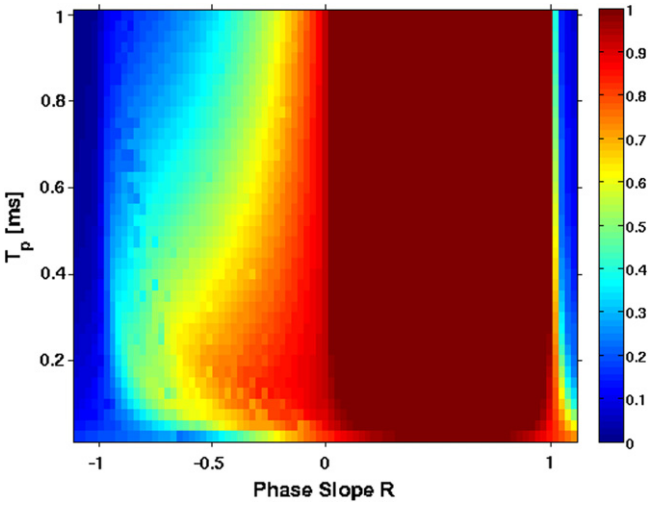

Fig. 10. The quality factor of Fig. 5D, which includes relaxation effects during each pulse, is divided by the signal intensity resulting from an ideal excitation pulse followed by relaxation for the equivalent time T_{evol} (see Fig. 8), as described in the text. This ratio is 1 for almost all positive R, showing there is no need to use relaxation-compensated pulses in the coherence transfer application of Fig. 8. To minimize T_{exc}, the largest R possible should be chosen together with the largest quality factor, independent of relaxation, as determined, for example, in Fig. 5A and B.

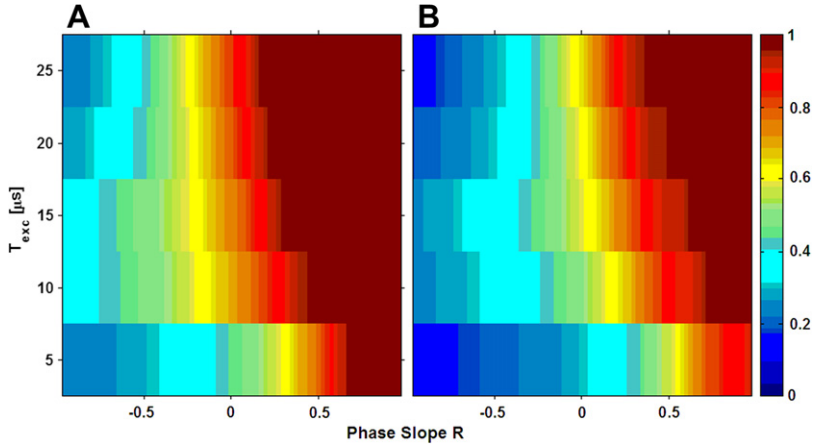

Fig. 9. Quality factor QF for optimal control pulses designed to uniformly excite a bandwidth $\Delta f = 50$ kHz is plotted as a function of T_{exc} (see Eq. (6)) and R ($-0.975 \leqslant R \leqslant 0.975$) for (A) $RF_{lim} = 15$ kHz and (B) $RF_{lim} = 10$ kHz. The color bar at the right of the figure provides the scale for QF. (For interpretation of the references to color in this figure legend, the reader is referred to the web version of this article.)

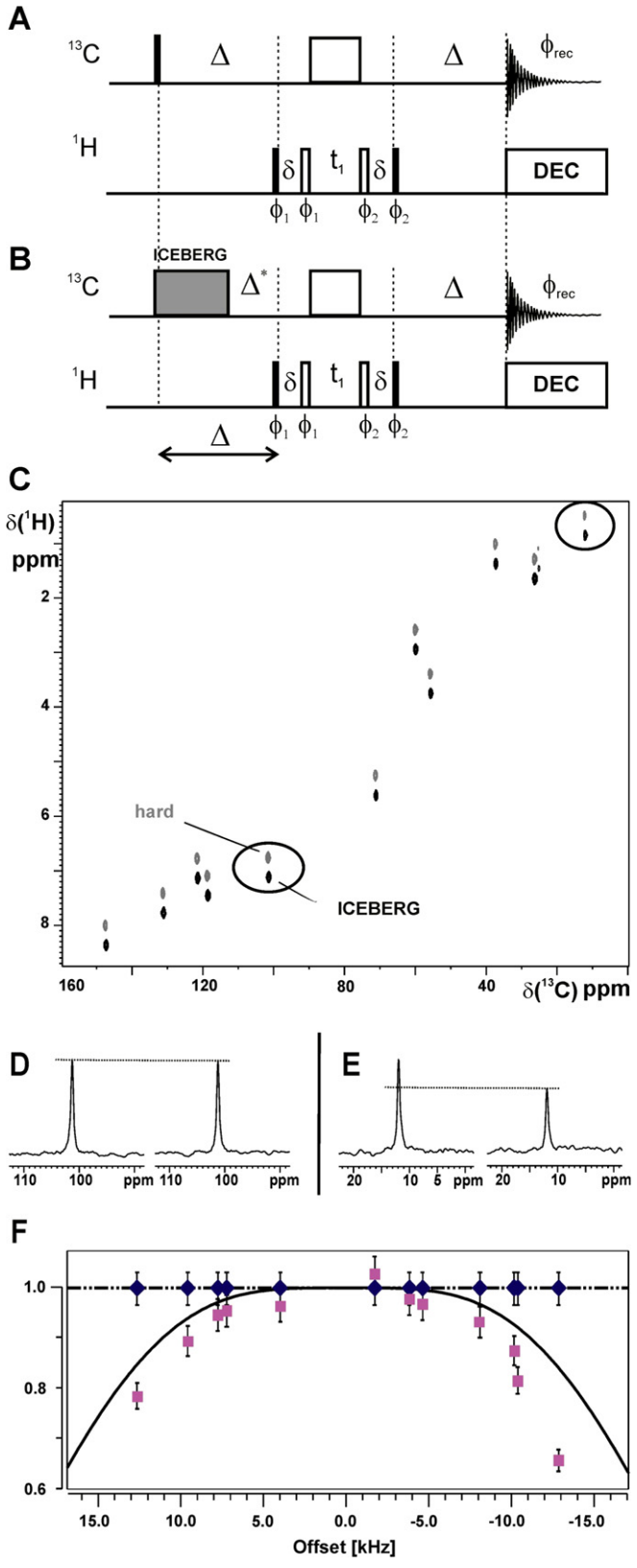

Fig. 11. Carbon excited and detected HMQC experiment using a conventional 90° hard pulse (A) and an ICEBERG pulse for excitation (B). The figure illustrates general broadband applications, such as ^{19}F or ^{31}P. Filled squares correspond to 90° pulses while open squares indicate 180° pulses, with the wide box on ^{13}C representing a refocussing pulse constructed out of two phase-modulated excitation pulses [6] using the principle described in Ref. [17]. Phases are x with the exception of $\phi_1 = x, -x$; $\phi_2 = x, x, -x, -x$; and $\phi_{rec} = x, -x, -x, x$. Delays are $\Delta = 1/(2^1J_{CH})$, with Δ^* reduced by the effective evolution period of the ICEBERG pulse, $R \cdot T_p$. Both experiments have practically identical overall sequence lengths but the offset-compensated ICEBERG HMQC provides higher sensitivity, especially at the edges of the carbon chemical-shift range. Experimental data acquired on hydroquinidine in $CDCl_3$ are shown in (C), with the ICEBERG HMQC cross peaks shown in black and the hard pulse version shown in gray with a slight shift in ^{1}H. Slices of the encircled cross peaks near $\delta(^{13}C) = 100$ ppm are compared in (D) for ICEBERG (left) and the hard pulse version (right). A similar comparison showing the loss off signal in the hard pulse version is shown in (E) near $\delta(^{13}C) = 12$ ppm. The experiment was implemented using a 1.4-28 ms ICEBERG pulse ($R = 0.95$, giving an effective contribution to the overall pulse sequence length of 1.428 ms · 0.05 = 71.4 μs) and a hard pulse of 35.7 μs duration. The simulation of the offset profiles of the ICEBERG (dash-dotted line) and hard 90° pulse (solid line) are shown in (F) together with the experimental signal intensities (ICEBERG HMQC signal intensities normalized to 1.0).

performed using ^{1}H excitation and detection, the large ^{13}C chemical-shift serves as a proxy for similar correlation experiments based on ^{19}F or ^{31}P excitation which will benefit from the ICEBERG scheme. These experiments, however, were not available to the authors.

HMQC performance using a 1.428 ms ICEBERG pulse ($R = 0.95$), optimized to achieve uniform excitation over the full carbon chemical-shift range, is compared to the same experiment using a 35.7 μs hard pulse (i.e., RF amplitude equal to the peak RF of the ICEBERG pulse). Embedding the ICEBERG pulse in the delay period results in an effective excitation pulse length $T_{exc} = 71.4$ μs, according to Eq. (6). Thus, the duration of the entire experiment is practically identical in both cases. However, in contrast to the ICEBERG version, which provides uniform excitation across the entire offset range, signal intensity in the hard pulse version is reduced by as much as 38% at the edges of the carbon chemical-shift range. Further details are provided in the figure caption.

The experiments were recorded on a Bruker Avance 750 MHz spectrometer using a triple resonance inversely detected room temperature probe head. 1024 × 128 data points were acquired with corresponding spectral widths of 200.8 ppm (^{13}C) and 8.5 ppm (^{1}H). Sixteen transients per increment gave an overall experiment time of 35 min for each of the two experiments.

6. Conclusion

The features of pulses which excite transverse magnetization with linear phase as a function of offset have been presented. A pulse with phase slope R at resonance offset ω produces a net chemical-shift evolution $R\omega T_p$ during a pulse of length T_p. Although pulses producing many functional forms $R(\omega)$ are possible, the focus here is on high performance pulses designed to produce constant phase slope R in the range $(-1, 1)$. Positive R pulses can provide significantly increased bandwidth for a given pulse length compared to BEBOPs requiring no phase correction, or shorter pulses for the same bandwidth. Uniform excitation over bandwidths which are a factor of 10 times the peak RF amplitude of the pulse are readily achievable. In addition, the linear phase evolution gives a J-coupling of RJ during the pulse. Large R then results in significant coupling evolution during the pulse, enabling the use of what might otherwise be prohibitively long pulses for coherence transfer. For $R < 0$, prefocused pulses are possible. Finally, pulses designed to mitigate relaxation effects require small R [8].

Acknowledgments

T.E.S. acknowledges support from NSF Grant CHE-0518174. B.L. thanks the Fonds der Chemischen Industrie and the Deutsche Forschungsgemeinschaft for support. S.J.G. acknowledges support from the Deutsche Forschungsgemeinschaft for Grant Gl 203/6-1, the

Fonds der Chemischen Industrie, and thanks the EU project Bio-DNP. N.K. acknowledges Darpa Grant F49620-0101-00556.

References

[1] E. Pinch, Optimal Control and the Calculus of Variations, Oxford University Press, Oxford, 1993.
[2] T.E. Skinner, T.O. Reiss, B. Luy, N. Khaneja, S.J. Glaser, Application of optimal control theory to the design of broadband excitation pulses for high resolution NMR, J. Magn. Reson. 163 (2003) 8–15.
[3] T.E. Skinner, T.O. Reiss, B. Luy, N. Khaneja, S.J. Glaser, Reducing the duration of broadband excitation pulses using optimal control with limited RF amplitude, J. Magn. Reson. 167 (2004) 68–74.
[4] K. Kobzar, T.E. Skinner, N. Khaneja, S.J. Glaser, B. Luy, Exploring the limits of broadband excitation and inversion pulses, J. Magn. Reson. 170 (2004) 236–243.
[5] T.E. Skinner, T.O. Reiss, B. Luy, N. Khaneja, S.J. Glaser, Tailoring the optimal control cost function to a desired output: application to minimizing phase errors in short broadband excitation pulses, J. Magn. Reson. 172 (2005) 17–23.
[6] T.E. Skinner, K. Kobzar, B. Luy, M.R. Bendall, N. Khaneja, S.J. Glaser, Optimal control design of constant amplitude phase-modulated pulses: application to calibration-free broadband excitation, J. Magn. Reson. 179 (2006) 241–249.
[7] C. Bauer, R. Freeman, R. Frenkiel, J. Keeler, A.J. Shaka, Gaussian pulses, J. Magn. Reson. 58 (1984) 442–457.
[8] N.I. Gershenzon, K. Kobzar, B. Luy, S.J. Glaser, T.E. Skinner, Optimal control design of excitation pulses that accommodate relaxation, J. Magn. Reson. 188 (2007) 330–336.
[9] S. Conolly, D. Nishimura, A. Macovski, Optimal control solutions to the magnetic resonance selective excitation problem, IEEE Trans. Med. Imaging MI-5 (1986) 106–115.
[10] J. Pauly, P. Le Roux, D. Nishimura, A. Macovski, Parameter relations for the Shinnar–Le Roux selective excitation pulse design algorithm, IEEE Trans. Med. Imaging 10 (1991) 53–65.
[11] D.E. Rourke, P.G. Morris, The inverse scattering and its use in the exact inversion of the Bloch equation for noninteracting spins, J. Magn. Reson. 99 (1992) 118–138.
[12] E. Kupce, R. Freeman, Polychromatic selective pulses, J. Magn. Reson. A 102 (1993) 122–126.
[13] D.E. Rourke, M.J.W. Prior, P.G. Morris, J.A.B. Lohman, Stereographic projection method of exactly calculating selective pulses, J. Magn. Reson. A 107 (1994) 203–214.
[14] J.W. Carlson, Exact solution for selective-excitation pulses: II. Excitation pulses with phase control, J. Magn. Reson. 97 (1992) 65–78.
[15] J.S. Waugh, Theory of broadband spin decoupling, J. Magn. Reson. 50 (1982) 30–49.
[16] M.H. Levitt, Composite pulses, in: D.M. Grant, R.K. Harris (Eds.), Encyclopedia of Nuclear Magnetic Resonance, vol. 2. John Wiley & Sons, Chichester, NewYork, Brisbane, Singapore, 1996, p. 1396.
[17] B. Luy, K. Kobzar, T.E. Skinner, N. Khaneja, S.J. Glaser, Construction of universal rotations from point to point transformations, J. Magn. Reson. 176 (2005) 179–186.